Large Eddy Simulation of Flow around a Bluff Body of Vehicle Shape

Dong-Sik Jang
Department of Mechanical Engineering, Graduate School of Pukyong National University, Busan 608-739, Korea
Yeon-Won Lee*
School of Mechanical Engineering, Pukyong National University, Busan 608-739, Korea
Deug-Hee Doh
Division of Mechanical and Information Engineering, Korea Maritime University, Busan 606-791, Korea
Toshio Kobayashi
Institute of Industrial Science, The University of Tokyo, Tokyo 106, Japan
Chang-Soo Kang
Professor Emeritus, Kyungpook National University, Daegu 702-701, Korea

The turbulent flow with wake, reattachment and recirculation is a very important problem that is related to vehicle dynamics and aerodynamics. The Smagorinsky Model (SM), the Dynamics Subgrid Scale Model (DSM), and the Lagrangian Dynamic Subgrid Scale Model (LDSM) are used to predict the three-dimensional flow field around a bluff body model. The Reynolds number used is 45,000 based on the bulk velocity and the height of the bluff body. The fully developed turbulent flow, which is generated by the driver part, is used for the inlet boundary condition. The convective boundary condition is imposed on the outlet boundary condition, and the Spalding wall function is used for the wall boundary condition. We compare the results of each model with the results of the PIV measurement. First of all, the LES predicts flow behavior better than the k-ε turbulence model. When we compare various LES models, the DSM and the LDSM agree with the PIV experimental data better than the SM in the complex flow, with the separation and the reattachment at the upper front part of the bluff body. But in the rear part of the bluff body, the SM agrees with the PIV experimental results better than them. In this case, the SM predicts overall flow behavior better than the DSM and the LDSM.

Key Words : Large Eddy Simulation, Smagorinsky Model, Dynamic Subgrid Scale Model, Lagrangian Dynamic Subgrid Scale Model, Particle Image Velocimetry

1. Introduction

Turbulence is a natural flow phenomena that we experience in our daily lives. Although it is impossible to get an exact solution of turbulence, we have tried to get an approximated solution by using computers. But the turbulent flow has random fluctuations, not only in space but also in time. So it is impracticable to predict accurately the turbulent flow with the most advanced computers. Recently, because of improvement of computers, the use of computational fluid dynamics that calculates approximated solution is more increased.

* Corresponding Author,
E-mail : ywlee@pknu.ac.kr
TEL : +82-51-620-1417; **FAX** : +82-51-620-1531
School of Mechanical Engineering, Pukyong National University, San 100, Yongdang-Dong Nam-Gu, Busan 608-739, Korea. (Manuscript **Received** September 3, 2001; **Revised** October 10, 2001)

The Direct Numerical Simulation (DNS), which calculates governing equations of the turbulent flow by the numerical method without any models, gives an exact solution to us. Because it takes about 2~640 years in calculating the flow of $Re=10^5\sim10^6$, it is not useful (Jung, 1994), and it is just used to check several turbulence models and to calculate simple flow of low Reynolds numbers. Thus, it is difficult to use the DNS. The LES comes true as an alternative method of the DNS, which is the mid-step of the Reynolds Averaging Navier-Stokes model (RANS) and the DNS. It calculates the Grid-Scale (GS) directly as the DNS method, and does the Subgrid-Scale (SGS) by modeling.

Theological justice of the LES is as follows: most turbulent energies are included in large scale flow systems, small scale flow is not concerned with direction effect by mean shear stress, and all physical quantities are not changeable, even coordinate is turned or reflected (Tennekes and Lumley, 1994). Therefore the LES is a more general method than RANS which considers all scales of the flow system, and is less dependent in shape. For these reasons, LES has become popular as numerical method of the turbulence flow.

Currently, the LES is being investigated by several researchers. Especially, Moin et al. (1982) applied the LES to turbulent channel flow, and compared numerical results with experimental results. Germano et al. (1991) proposed the DSM to overcome the defect of the SM which didn't have universality of the model coefficient. Also, Ferziger et al. (1996) applied the LES to the flow field around a cube mounted on one wall of a channel, and they confirmed the horseshoe vortex, the swirling flow, the arch vortex, etc.

Kobayashi et al. (1989) performed the numerical analysis of a flow field around a two-dimensional road vehicle in order to compare results of the LES with results of k-ε turbulence model. They reported that the LES agreed with experimental result more than the k-ε turbulence model. Also, Murakami et al. (1990) preformed the numerical analysis and wind tunnel test, so as to compare results of the LES with those of the k-ε turbulence model about the turbulent structure around a cube.

In Korea, Yang (1994) performed the LES of the turbulent flow in channel with a two-dimensional obstacle, and Choi et al. (1997) performed the LES in order to analyze far field noise.

Sohankar et al. (2000) performed the LES of flow past a square cylinder, and they proposed the one-equation DSM because the DSM predictions were too large, more than SM and experimental results.

Morinish et al. (2000) researched effects of the order of accuracy of finite difference scheme and those of the grid resolutions on LES. In the case of insufficient accuracy of a finite difference scheme, they suggested that SM with damping function predicts the flow behavior better than DSM.

In this study, we compare results of the k-ε turbulence model and several LES models(SM, DSM and LDSM) with those of PIV experiment about bluff body which is the most simplified shape of moving vehicles.

2. Governing Equations

The governing equations of the k-ε turbulence model are eliminated because they are well known to us.

The LES calculates the Grid-Scale (GS) fluid motions that can be resolved by the computation grid directly, but it models only the Subgrid-Scale (SGS) fluctuations that are smaller than the grid resolution. For the incompressible flow, the governing equations of the turbulent flow are described as follows.

Continuity equation:

$$\frac{\partial \bar{u}_i}{\partial x_i}=0 \tag{1}$$

Navier-Stokes equation:

$$\frac{\partial \bar{u}_i}{\partial t}+\frac{\partial \bar{u}_i\bar{u}_j}{\partial x_j}=-\frac{\partial \bar{p}}{\partial x_i}+\nu\frac{\partial^2 \bar{u}_i}{\partial x_j^2}+\frac{\partial \tau_{ij}}{\partial x_j} \tag{2}$$

where the over bar $(-)$ denotes the filtered values in the grid resolution space. The last term, τ_{ij} in the Navier-Stokes equation represents the SGS stress that is defined by a SM as follows.

$$\tau_{ij}=\overline{u_iu_j}-\bar{u}_i\bar{u}_j=\nu_{SGS}\bar{S}_{ij} \quad (3)$$
$$\nu_{SGS}=(C_s\Delta)^2|\bar{S}|$$

Here, $\bar{S}_{ij}$ and $|\bar{S}|$ are a strain rate and its norm, and described as follows,

$$\bar{S}_{ij}=\frac{1}{2}\left(\frac{\partial\bar{u}_i}{\partial x_j}+\frac{\partial\bar{u}_j}{\partial x_i}\right) \quad (4)$$
$$|\bar{S}|=\sqrt{2\bar{S}_{ij}\bar{S}_{ij}} \quad (5)$$

The Smagorinsky coefficient $C_s=0.1$ is adopted, and the Δ denotes a filter width that is calculated from the mesh size. The Van Direst type damping function is adopted to reduce the length scale in the near wall region.

$$\Delta=f(\Delta_1\Delta_2\Delta_3)^{1/3} \quad (6)$$
$$f=1-\exp\left(-\frac{y^+}{25}\right) \quad (7)$$

On the other hand, it is difficult to determine optimum Cs to reflect closely the state of flow, therefore, Germano et al. (1991) proposed the DSM to overcome the defect of the SM.

According to Germano et al. , after the test scale filter denoted by tildes symbol ($\sim$) is operated, a test scale filtered SGS stress also yields.

$$T_{ij}=\widetilde{\overline{u_iu_j}}-\tilde{\bar{u}}_i\tilde{\bar{u}}_j \quad (8)$$

Now, if the same model, such as the Smagorinsky model, is applied to the two SGS stresses (T_{ij} and τ_{ij}), unknown values of the model coefficient ($C=C_s^2$) can be dynamically determined. Lilly (1992) proposed the following equations;

$$C=-\frac{1}{2\Delta^2}\frac{L_{ij}M_{ij}}{M_{ij}M_{ij}} \quad (9)$$

$$L_{ij}=\widetilde{\bar{u}_i\bar{u}_j}-\tilde{\bar{u}}_i\tilde{\bar{u}}_j-\frac{1}{3}\delta_{ij}L_{kk} \quad (10)$$

$$M_{ij}=\alpha^2(|\tilde{\bar{S}}|\tilde{\bar{S}}_{ij}-\widetilde{|\bar{S}|\bar{S}_{ij}}) \quad (11)$$

$$\alpha=\frac{\tilde{\bar{C}}_s\tilde{\bar{\Delta}}}{C_s\Delta} \quad (12)$$

And, Meneveau et al. (1994) proposed the LDSM that calculates model coefficient by considering the pathline of fluid flow. Therefore, the LDSM can be applied to complex shapes because averaging over homogeneous directions is unnecessary.

$$C=-\frac{1}{2\Delta^2}\frac{I_{LM}}{I_{MM}} \quad (13)$$

$$\frac{\partial I_{LM}}{\partial t}+u_j\frac{\partial I_{LM}}{\partial x_j}=\frac{1}{T}(L_{ij}M_{ij}-I_{LM}) \quad (14)$$

$$\frac{\partial I_{MM}}{\partial t}+u_j\frac{\partial I_{MM}}{\partial x_j}=\frac{1}{T}(M_{ij}M_{ij}-I_{MM}) \quad (15)$$

where,

$$T=C_t\Delta I_{LM}^{-1/4} \quad (16)$$

The C_t parameter used is 2.0 which is recommended by Meneveau et al (1994). Also, if C is equal to a minus value, then C is equal to zero for stability of the calculation.

3. Numerical Method

In this calculation, the LES and the k-ε turbulence model are applied and performed on the numerical simulation of the turbulent flow around the bluff body of vehicle shape.

For the discretization of the governing equations, the finite volume method (FVM) is adopted for both simulations. A staggered grid is used for removing oscillations of pressure field.

In the k-ε turbulence model, the hybrid difference scheme is used for the convection term, and second order central difference scheme is used for the diffusion term. The SIMPLE algorithm is used for the simultaneous iteration method for pressure and velocity. In the LES, second order central difference scheme is used for the convection and diffusion terms, and the third order Runge-Kutta method is employed to advance in time. The SMAC method is used for the simultaneous iteration method.

The fully developed turbulent flow, which is generated by the driver part, is used for the inlet boundary condition. The driver part is simultaneously calculated with the main part. The outlet condition is applied in the convective boundary condition in the case of LES (Park, et al. , 1997)

$$\frac{\partial u_i}{\partial t}+U_c\frac{\partial u_i}{\partial x}=0 \quad (17)$$

where, the value of U_c is equal to the mean velocity of the main flow.

The Spalding wall function is used for the wall boundary condition in the case of the LES and

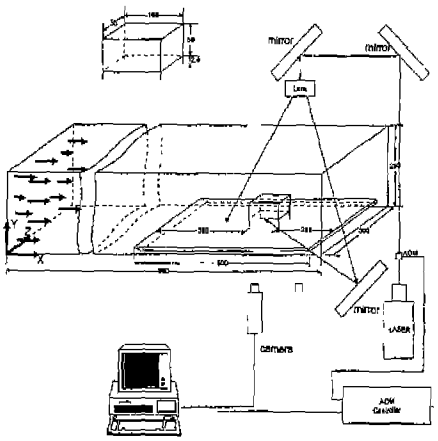

Fig. 1 Schematic of PIV system

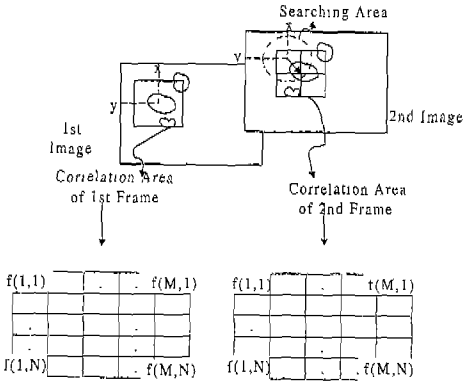

Fig. 2 Principle of the gray level cross-correlation PIV

the log-law wall function is applied for the case of the k-ε turbulence model.

The cyclic boundary condition is used in the spanwise direction and the free slip condition is used for the upper boundary condition.

The time increment is $\Delta t=0.01$. After the flow is fully developed, each simulation is averaged for 1000.0 seconds.

4. Principle and Experimental Method of the PIV

Figure 1 shows the overall experimental apparatus. The size of the aluminum-based model of the bluff body is 50mm×50mm×100mm. This model is suspended with four thin pins in a circulating water channel (1100mm×300mm×250mm). The small tracers (Nylon, s. g. 1.02) were put into the channel.

The light from an Ar-ion laser (500mW) passes through a probe to make two-dimensional light sheet. In order to make coded images of the tracer particles on one frame, the AOM (Acoustic-Optical Modulator) was used. It plays as an optical chopper for the laser light source like electric shutter of the conventional camera.

The AOM controller is synchronized with the camera and sends a carrier signal to the AOM unit with 100MHz, which enables the AOM system to work as an electric shutter.

The images taken through the camera are aptured with a frame grabber (Ditect, DT64) and converted into 8 bits levels (255) on the host computer (IBM, Pentium 400MHz).

In order to get velocity vectors, a process for particle identification is done for the extraction of velocity vectors. This is based upon the two-fields cross-correlation method, in which the coordinate indicating the maximum coefficient is assumed to be a vector terminal point (Kimura et al., 1986, Utami and Blackwelder, 1991). Figure 2 shows a schematic picture for the gray level cross-correlation. The searching area is the maximum allowable distance between the grid point of the first image and the terminal point of the second image. The gray levels of the whole pixels in the correlation area of the first and of the second images are cross-correlated within the searching area. Equation (18) is a formula to calculate the cross-correlation coefficients.

$$C_{fg}=\frac{\sum_{i=1}^{n^2}(f_i-\bar{f}_i)(g_i-\bar{g}_i)}{\sqrt{\sum_{i=1}^{n^2}(f_i-\bar{f}_i)^2\sum_{i=1}^{n^2}(g_i-\bar{g}_i)^2}} \tag{18}$$

Here, f_i and g_i mean gray levels of the pixels within the correlation region and, over bar $(-)$ these letters indicates the average value of the gray levels of the pixels within the correlation region. And n^2 means the pixel number of the correlation area. The terminal point of the velocity vector is decided when the calculated coefficient is the maximum value in the searching area. In order to get the velocity vector data, pre-process is needed

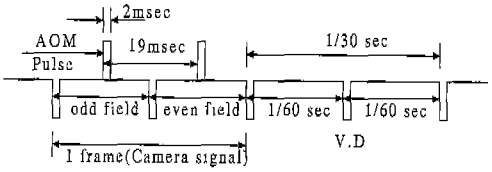

Fig. 3 Relations between NTSC (camera signal) and AOM signals

before velocity vector acquisition for more accurate results. And a post process is needed for more easy understanding for the obtained raw data. The grabbed frame image is separated into two fields, odd and even fields. The velocity vectors are obtained on the two field images by using the PIV algorithm mentioned above. The time difference of the field image is 20msec which is adjustable by using the AOM controller. Figure 3 shows the time relation between the AOM pulse signal and the NTSC camera signal. The pulse signal for AOM is activated twice, the one is in the odd field of a frame and the other is in the even field of the same frame with the same pattern.

Therefore, two particle images are pictured for one particle on one frame. The digitized images are stored with 256 gray levels in integer values and these values are transformed into ASCII files for image processing. Positional data on each pixel on the 2-dimensional image are produced and its gray level distribution is obtained from the image files. During the pre-processing the most important thing is to eliminate the noise that affects greatly the reliability for the resulted velocity vectors.

In this study, it was verified empirically that the median filter was superior to other filters to reduce the noise. However, a more effective method in reducing the noise was to eliminate the background image from each image to be processed. In this study, the background image is obtained by averaging about 200 consecutive field images and this image is subtracted from the actual field images to be processed.

The calculating time on the host computer was about 1 minute when the grid for velocity vector extraction was set to 60×60, the radius for the

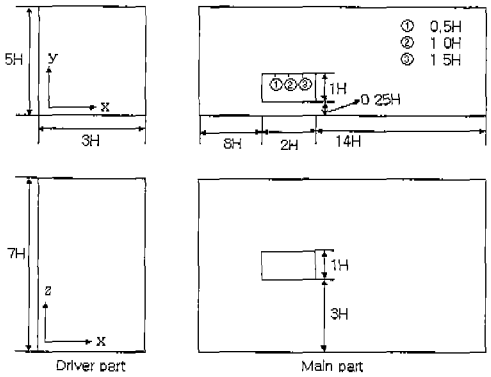

Fig. 4 Computational Domain

searching area was set to 20 pixels, the size for the correlation area was set to 32×32 pixels. Since there is an positional uncertainty with maximum ±1 pixel when the terminal point of the velocity vector is obtained by the PIV based on pixel resolution, the sub-pixel interpolation method (Utami and Blackwelder, 1991) is adopted for more accurate calculation. Further, there might be some erroneous vectors depending on the size of correlation area and the distance of the searching area. Therefore, an error vector elimination method (Hojo and Takashima, 1995) based on the continuous flow condition was adopted.

5. Results and Discussion

The computational domain, shown in Fig. 4, is composed of the driver part and the main part. The calculation region of the driver part is $3H\times5H\times7H$ and the grid numbers are $49,920(20\times48\times52)$, however the computational domain of the main part is $20H\times5H\times7H$ and the grid numbers are 189, $696(76\times48\times52)$. The Reynolds number is 45, 000 based on the bulk velocity and the height of the bluff body.

Figure 5 shows the mean velocity at the center plane of the bluff body. Figure 5(a) shows the occurrence of the separation and the recirculation flows in the upper bluff body, and Fig. 5(b), (c) and (d) show the same results. But the reattachment point of the SM occurs that of the

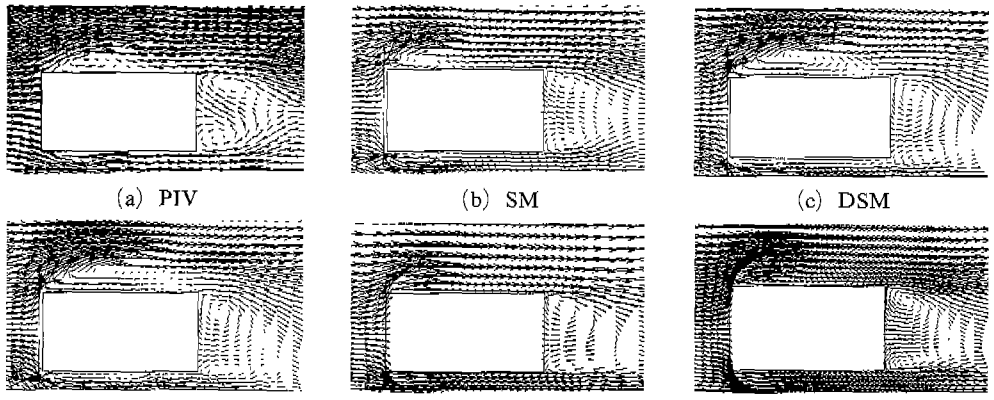

(a) PIV (b) SM (c) DSM

(d) LDSM (e) k-ε(coarse) (f) k-ε(fine)

Fig. 5 Distribution of mean velocity vectors at the center plane

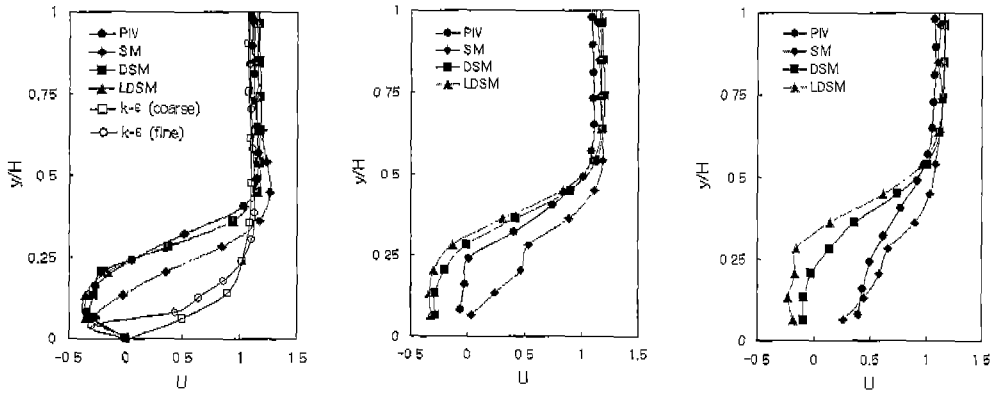

(a) x=0.5H (b) x=1.0H (c) x=1.5H

Fig. 6 Profiles of the mean velocity U at the center plane

PIV experimental result. And the predictions of the recirculation flow in Fig. 5(c) and (d) are too large, so the flow is reattached behind that of the PIV experimental result. But in Fig. 5(e), the recirculation flow doesn't occur in the upper bluff body. On the other hand, in Fig. 5(f), though the recirculation flow occurs in the upper bluff body, the size is smaller than those of the PIV and LES models. And in the wake region, Fig. 5(c) and (d) predict a smaller vortex which is made in the lower part. In Fig. 5 (c) and (d), the predictions of the recirculation flow which are large, and the reattachment occurs behind that of the result of the SM.

Figure 6 shows the profiles of the mean velocity U of the upper center plane at the positions of 0. 5H, 1.0H and 1. 5H. In Fig. 6(a), the DSM and the LDSM agree with the PIV better than the SM. In Fig. 6(c), however, the SM agrees with the PIV better than the DSM and the LDSM, and the LDSM predictions are larger than the DSM. On the other hand, in the case of k-ε turbulence model with coarse gird, the separation and the recirculation flow don't occur. In the case of k-ε turbulence model with fine grid, though the recirculation flow occurs, its size is much smaller than size of the PIV and the LES models.

Figure 7 shows the distribution of turbulent kinetic energy production P_k. The k-ε turbulence model, by introducing eddy viscosity model, always generates positive values as shown in Eq. (19). Hence, the values of turbulent kinetic energy production given by the k-ε turbulence model become very large as compared with the LES.

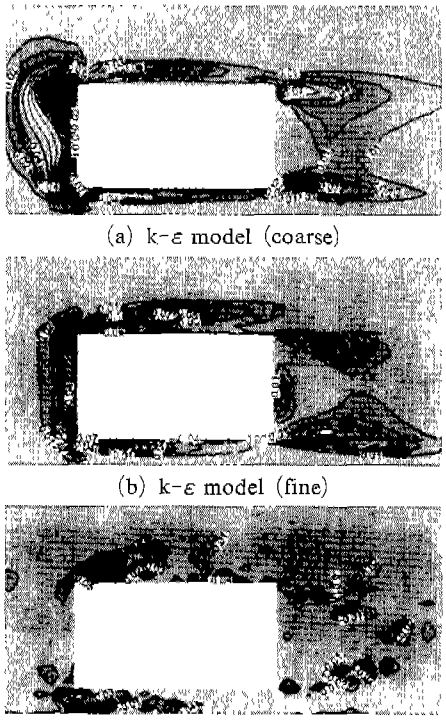

(a) k-ε model (coarse)

(b) k-ε model (fine)

(c) SM

Fig. 7 Distribution of turbulent kinetic energy production P_k

But, in the case of the LES, the value of turbulent kinetic energy production may become positive or negative, according to the flow condition as defined in Eq. (20) which is the original form.

k-ε turbulence model

$$P_k \cong \nu_t \frac{\partial u_i}{\partial x_j}\left(\frac{\partial u_i}{\partial x_j}+\frac{\partial u_j}{\partial x_i}\right) \tag{19}$$

LES

$$P_k = -u_i' u_j' \frac{\partial u_i}{\partial x_j} \tag{20}$$

In Fig. 7(c), negative values of P_k appear nearby the reattachment point on the upper surface of the bluff body and at wake region. This point shows the clear difference between LES and the k-ε turbulence model.

Figure 8 shows the profile of the time-averaged mean velocity U of the upper center plane of the bluff body at y=0.06438H position, to x-direction. In the case of the PIV, the flow is recovered at 1.1H. In the case of the SM, the flow is

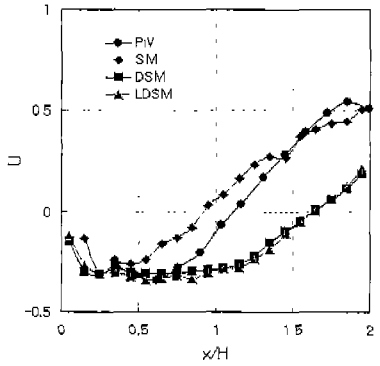

Fig. 8 Profiles of mean velocity U of the upper center plane of bluff body at y=0. 06438H

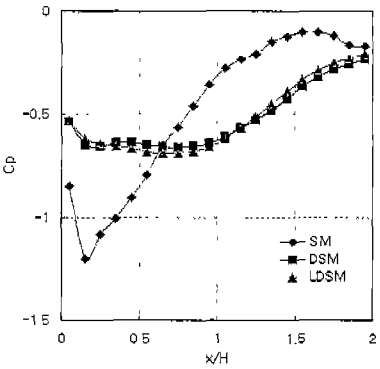

Fig. 9 Profiles of pressure coefficient Cp at the upper center plane of the bluff body

recovered before 1H because the recirculation flow is less predicted. The prediction of the DSM and the LDSM of the recirculation flow is too large, so the flow is reattached at 1.6H.

Figure 9 shows the profiles of pressure coefficient C_p. In the case of the SM, pressure drop by separation occurs heavily in the upper front part, but the pressure is recovered rapidly. However, pressure drops of the DSM and the LDSM occur lower than that of the SM, and pressure recoveries of them occur smoothly.

Figure 10 shows the pressure contour at the center plane of the bluff body. At the upper front part with the separation and the recirculation flow, the DSM and the LDSM predicted more widely than the SM, because their predictions of the recirculation flow is too large. At the stagnation region, the DSM predicts higher than the SM and the LDSM.

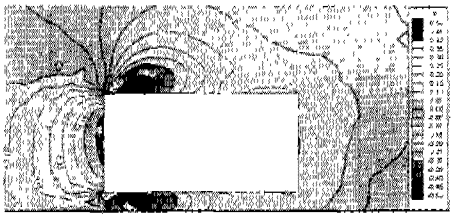

(a) SM

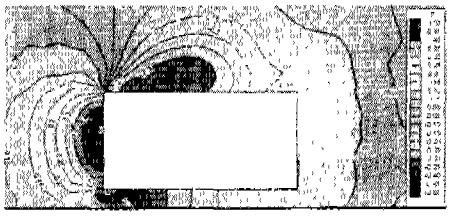

(b) DSM

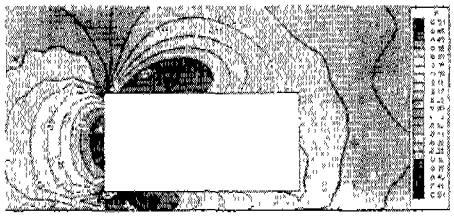

(c) LDSM

Fig. 10 Distribution of pressure contour at center-plane of the bluff body

Table 1 Drag coefficient, C_d

Models	Drag Coefficient
k-ε	1.058
SM	0.834
DSM	0.928
LDSM	0.841

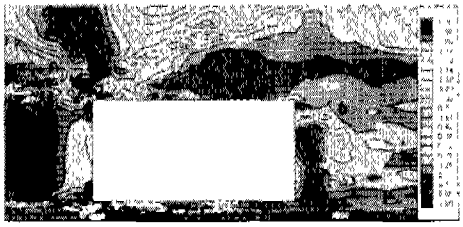

(a) DSM

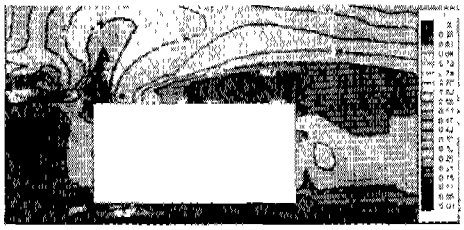

(b) LDSM

Fig. 11 Distribution of time-averaged model coefficient $C^{1/2}$ at the center plane

In the case of the drag coefficient C_d, several researchers reported that the k-ε turbulence model predicts C_d excessively. Especially, Myong et al. (1996, 1997) reported that certain k-ε turbulence model, which depends on the turbulence model and the finite difference scheme, predicted C_d about twice as large as the experimental data. So, it is necessary to find a way to overcome the defect of the k-ε turbulence model.

Table 1 shows the values of C_d that are simulated by several turbulence models. As you see, the k-ε turbulence model is 1.058, the SM is 0.834, the DSM is 0.928, and the LDSM is 0.841. The k-ε turbulence model predicts C_d bigger than any other LES models and the DSM prediction C_d is too large in comparison with the SM and the LDSM. This is because DSM predicts the pressure of the stagnation region higher than the SM and the LDSM.

Figure 11 shows the root mean model coefficient C. Generally, C is calculated higher than the SM (0.1). And Fig. 11 (a) shows a lower profile than Fig. 11 (b) at the reattachment part. It is considered that this factor affects the recirculation and the reattachment.

After this, continued research needs to be done on the Reynolds stress term, the secondary flow and effects of the grid dependence.

6. Conclusions

In this study, we compare results of the LES models and the k-ε turbulence model with those of the PIV on the flow around the bluff body of vehicle shape. The following conclusions are derived

(1) In the recirculation flow region at the upper part of the bluff body, the LES agrees with PIV experimental results better than the k-ε turbulence model.

(2) In the prediction of the C_d, it is judged that the LES will agree with the PIV experimental results better than the k-ε turbulence model.

(3) In the front upper part of the bluff body, the results of the DSM and the LDSM agree with those of the PIV experimental results. However, in the rear upper part of the bluff body, the results of the SM agree with those of the PIV experimental results.

(4) The DSM and the LDSM predict a model coefficient C larger than the SM.

(5) In this calculation, the SM agrees with the PIV experimental results better than the DSM and LDSM overall.

Acknowledgement

This work was financially supported by the Brain Korea 21 project (2001, RA).

References

Choi, H. C., Choi, M. R. and Kang, S. H., 1997, "A study on the Early Stage of a Transitional Boundary Layer and Far Field Noise Using a Large Eddy Simulation Technique," *Transactions of the KSME* (B), Vol. 25, No. 7, pp. 779~792.

Ferziger, J. H. and Peric, M., 1996, "Computational Methods for Fluid Dynamics," *Springer*, pp. 257~267.

Germano, M., Piomelli, U., Moin, P. and Cabot, W. H., 1991, "A Dynamic Subgrid-Scale Eddy Viscosity Model," *Phs. Fluids* A 3(7), pp. 1760~1765.

Hojo, K. and Takashima, H., 1995, "Detection of Erroneous Velocity Vectors Obtained in PIV," *J. of Visualization Society of Japan*, Vol. 15, Suppl. No. 2, pp. 177.

Jung, M. G., 1994, "Computational Turbulent Models," *J. of KSME*, Vol. 38, No. 3, pp 688~694.

Kimura, I., Takamori, T. and Inoue, T., 1986, "Image Processing Instrumentation of Flow by Using Correlation Technique," *Flow Visualization*, Vol. 6, No. 22, pp. 105.

Kobayashi, T., Kitoh, K. and Morinishi, Y., 1989, "Numerical Simulation on the Flow Around a Road Vehicle: a Comparison Between Numerical Results of LES and k-ε Model," *J. of Institute of Industrial Science*, Univ. of Tokyo, Vol. 41, No. 1, pp. 60~63.

Lilly, D. K., 1992, "A Proposed Modification of the Germano Subgrid-Scale Closure Method," *Phys. Fluids* A 4 (3), pp. 633~635.

Meneveau, C., Lund, T. S. and Cabot, W., 1994, "A Lagrangian Dynamic Subgrid-Scale Model for Turbulence," *Proceedings of the Summer Program* (Center for Turbulence Research), pp. 1~29.

Moin, P. and Kim, J., 1982, "Numerical Investigaion of Turbulent Channel Flow," *J. Fluid Mech.*, Vol. 118, pp. 341~377.

Morinishi, Y., Ichikawa, A., Okumura, T. and Nakabayashi, K., 2000, "Effects of the Order of Accuracy of Finite-Difference Method and Resolution on LES of Wall Turbulence," *J. of JSME* (B), Vol. 66, No. 647, pp. 1750~1757.

Murakami, S., Mochida, A. and Hayashi, Y., 1990, "Examining the k-ε Model by Means of a Wind Tunnel Test and Large-Eddy Simulation of the Turbulence Structure Around a Cube," *J. of Wind Eng. and Ind. Aerodynamics*, Vol. 35, pp. 87~100.

Myong, H. K., Park, H. K. and Jin, E., 1996, "Simulation of Three-Dimensional Turbulent Flows Around an Ahmed Body (Evaluation of Finite Differencing Schemes)," *Transactions of the KSME* (B), Vol. 20, No. 11, pp. 3589~3597.

Myong, H. K., Jin, E., Park, H. K., 1997, "Simulation of Three-Dimensional Turbulent Flows Around an Ahmed Body (Evaluation of Turbulence Models)," *Transactions of the KSME* (B), Vol. 21, No. 7, pp. 873~881.

Park, N. S., Kobayashi, T. and Taniguchi, N., 1997, "LES of Turbulent Flow Around a Surface-Mounted Cubical Obstacle in a Channel Using Lagrangian Dynamic SGS Model," *J. of Institute of Industrial Science*, Univ. of Tokyo, Vol. 49, No. 1, pp. 50~53.

Sohankar, A., Davidson, L. and Norberg, C., 2000, "Large Eddy Simulation of flow Past a Square Cylinder: Comparison of Different Subgrid Scale Models," *Transactions of the*

ASME, J. of Fluids Eng., Vol. 122, pp. 39~47.

Su, M. D., and Friedrich, R., 1994, "Investigation of Fully Developed Turbulent Flow in a Straight Duct with Large Eddy Simulation," *Transactions of the ASME, J. Fluid Eng.*, Vol. 116, pp. 677~684.

Tennekes, H. and Lumley, J. L., 1973, "A First Course in Turbulence," *MIT Publishing Company*, pp. 64~65.

Utami, T., Blackwelder, R., 1991, "A Cross Correlation Technique for Velocity Field Extraction from Particulate Visualization," *Exp. In Fluids*, Vol. 10, pp. 213~223.

Yang, K. S., 1994, "Large Eddy Simulation of Turbulent Flows," *J. of KSME*, Vol. 38, No. 3, pp. 688~694.